

Conformational statistics of randomly-branching double-folded ring polymers

Angelo Rosa*

Sissa (Scuola Internazionale Superiore di Studi Avanzati), Via Bonomea 265, 34136 Trieste, Italy

Ralf Everaers†

*Université de Lyon, ENS de Lyon, UCBL, CNRS,
Laboratoire de Physique and Centre Blaise Pascal, Lyon, France*

(Dated: July 18, 2021)

The conformations of topologically constrained double-folded ring polymers can be described as wrappings of randomly branched primitive trees. We extend previous work on the tree statistics under different (solvent) conditions to explore the conformational statistics of double-folded rings in the limit of tight wrapping. In particular, we relate the exponents characterizing the ring statistics to those describing the primitive trees and discuss the distribution functions $p(\vec{r}|\ell)$ and $p(L|\ell)$ for the spatial distance, \vec{r} , and tree contour distance, L , between monomers as a function of their ring contour distance, ℓ .

I. INTRODUCTION

Topologically constrained ring polymers often adopt double folded configurations characterized by a randomly branched primitive tree [1–7] (Figure 1(a)). In analogy to protein or RNA structures [8], such rings can be discussed in terms of a primary, a secondary, and a tertiary structure. The primary structure is simply defined through the connectivity of the ring monomers. The secondary structure arises from the double folding. Its characterisation comprises information on the mapping of the ring onto the graph as well as on the connectivity of the graph representing the primitive tree. Important characteristics are the contour distances, L , between tree nodes or the weight, N_{br} , of branches separated from the tree by severing a link. Finally, the tertiary structure defines the embedding of the rings and trees into (three dimensional) space. Relevant observables are the spatial distance, \vec{r} , between ring monomers or tree nodes, or the overall gyration radius, R_g .

As customary in polymer physics [9, 10], the tree behavior can be analyzed in terms of a small set of exponents describing how expectation values for these observables vary with the weight, N , of the trees or the contour distance, L , between nodes. Flory theory [4, 11–14] provides a useful framework for discussing the *average* behavior of a wide range of interacting tree systems beyond the small number of available exact results [15–17]. Furthermore, we have recently shown that the non-Gaussian distribution functions for tree observables are often of the Redner-des Cloizeaux (RdC) form and characterized by a small set of additional exponents, which can often be related to each other and the standard trees exponents [18].

Here we take a step back to the original polymer problem and consider rings, which are tightly wrapped around trees (Fig. 1(b)). “Navigating” on the tree along

a wrapped ring mixes the two concepts invoked above for characterizing trees: (i) the branching statistics controls how fast the mean contour distance on the tree grows with the contour distance between monomers along the ring and (ii) spatial distances depend on the conformations of paths on the tree in the embedding space. We consider ensembles of trees as described in our earlier works [18–20], namely: single self-avoiding trees in three dimensions and melts of trees in two and three dimensions. As a reference, we also consider the case of double-folded rings on conformations of *ideal* trees, *i.e.* without volume interactions. Specifically, we tightly wrap ring polymers around tree conformations we generated in our previous Monte Carlo simulations and explore the relation between the tree and the ring exponents.

The paper is organized as follows: In Section II, we define the tight wrapping of a tree by a ring and briefly review definitions and the theoretical background. We provide no explicit Methods section as there are no particular algorithmic difficulties associated to the wrapping process or the data analysis. The reader will instead find a concise introduction to the Monte Carlo methods used for generating lattice tree conformations and to the computational procedures for estimating scaling exponents and more numerical details in the Appendices at the end of the paper. We present and discuss results in Section III and conclude in Section IV.

II. DEFINITIONS AND BACKGROUND

A. Topologically constrained ring polymers

The transient folding of ring polymers subject to topological constraints (Fig. 1(a)) can be understood by using the analogy to randomly branched structures with annealed connectivity [1–5, 19–21]. A typical example is the one of a single ring in an array of fixed obstacles [1–3] which represents a theoretical model for the problem of a ring moving through a gel [22]. Furthermore, sev-

*Electronic address: anrosa@sissa.it

†Electronic address: ralf.everaers@ens-lyon.fr

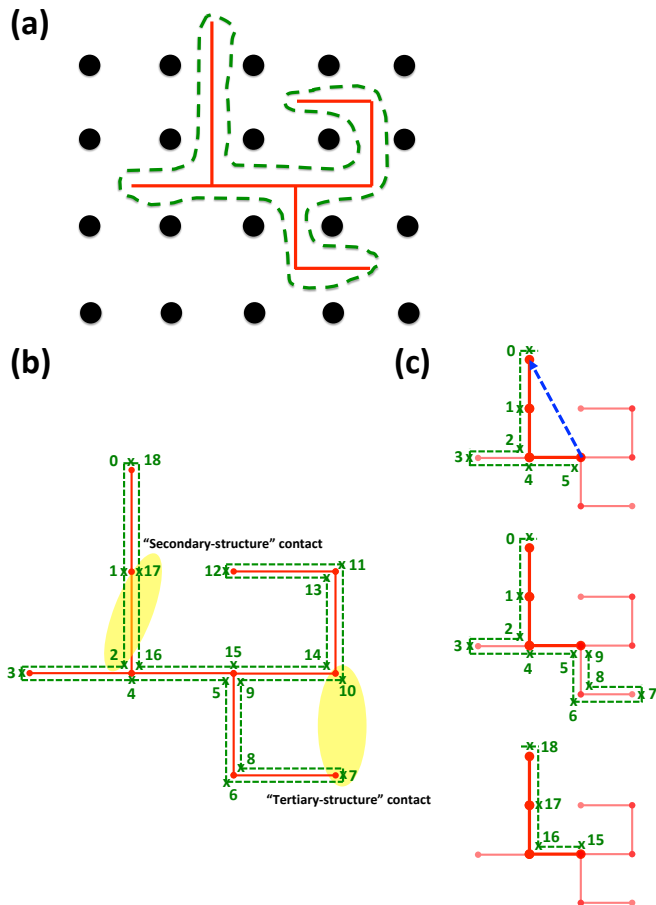


FIG. 1: (a) Ring polymers (green dashed line) in an array of fixed obstacles (and, in concentrated solutions and melt) adopt spatial conformations whose primitive paths (red solid line) can be mapped to randomly branched polymers with annealed connectivity. (b) Double-folded ring polymer (green dashed line) from a branched polymer (red solid line) of $N = 9$ bonds. The numbers indicate the contour distance of the ring (in units of elementary bonds) measured from one arbitrarily chosen end of the branched polymer. The pairs of node (2, 17) and (7, 10) are classified as “secondary-” and “tertiary-structure” contacts, respectively. (c) Ring contour distances $\ell = 5, 9, 3$ (dashed green lines, top to bottom) compatible with the tree contour distance $L = 3$ (thick red line) and spatial distance $|\vec{r}|$ (blue arrow).

eral authors have suggested that the same analogy may be applied to describe spatial conformations of unknotted and untangled ring polymers in melts [1, 3, 23, 24] and chromosomes in eukaryotes [25–28]. Although it remains a non-trivial question, if [23] or to which extent [3, 24, 29, 30] the link to the melts can be pushed forward, we have shown [5] that it provides at least an excellent approximation.

In this work, we consider double-folded ring polymers on lattice branched structures taken from different ensembles: $3d$ trees in good solvent conditions *i.e.* with purely repulsive interactions between tree nodes, and $2d$ and $3d$ melt of trees which are relevant to the problem of

untangled polymers in dense solution. For comparison, we also study single ring conformations whose branched primitive paths are generated under ideal conditions *i.e.* without excluded volume effects between tree nodes.

B. Rings, trees, notation and units

We measure energy in units of $k_B T$ and length in units of the Kuhn length, l_K , of the ring polymer. There are two oppositely oriented ring segments associated to each tree segment. As a consequence, there are $2N$ ring segments for a tree composed of N segments. This corresponds to $N + 1$ nodes for the tree and $2N + 1$ nodes for the ring. To see that it is possible to characterize the primitive trees and the rings by the same Kuhn length, consider the limit of a small double-folded ring of contour length $\ell_{ring} \equiv 2N$ corresponding to an unbranched primitive chain. The gyration radius of the latter is given by $R_g^2 = l_K(\ell_{ring}/2)/6 = l_K \ell_{ring}/12$, corresponding to a closed random walk [5].

We use the letters N and N_{br} to denote the number of segments of a tree or a branch, respectively. The symbols L and ℓ are reserved for contour lengths on the tree and the ring, respectively. Spatial distances are denoted by the letters R and r . Examples are the tree gyration radius, R_g and spatial distances between nodes, \vec{r}_{ij} .

A wrapping introduces an additional metric on the embedded graph, *i.e.* two nodes I and J can be characterized by their spatial distance, $\vec{r}_{IJ} = \vec{r}_I - \vec{r}_J$, their contour distance, $L_{IJ} \leq \ell_{IJ} \leq N$, on the ring. In the following, we substitute the arbitrary labelling $0 \leq I, J \leq N$ of the tree nodes by the (primary structure) ring labels $0 \leq i, j \leq 2N$ such that $\ell_{ij} \equiv \text{mod}(|i - j|, N)$. Furthermore, we distinguish between secondary structure contacts on the tree and tertiary structure contacts occurring in a particular tree conformation in the embedding space. Figure 1(c) illustrates $|\vec{r}_{ij}|$ (blue arrow), L_{ij} (thick red line) and the corresponding ℓ_{ij} 's (dashed green lines) for an example.

C. Randomly branching trees

A small set of exponents describes how expectation values for observables characterising tree connectivities and conformations vary with the weight, N , of the trees or the contour distance, L , between nodes:

$$\langle N_{br}(N) \rangle \sim N^\epsilon \quad (1)$$

$$\langle L(N) \rangle \sim N^\rho \quad (2)$$

$$\langle R^2(L) \rangle \sim L^{2\nu_{\text{path}}} \quad (3)$$

$$\langle R_g^2(N) \rangle \sim N^{2\nu} \quad (4)$$

Here, $\langle N_{br}(N) \rangle$ denotes the average branch weight; $\langle L(N) \rangle$ the average contour distance or length of paths on the tree; $\langle R^2(L) \rangle$ the mean-square spatial distance between nodes with fixed contour distance; and $\langle R_g^2(N) \rangle$

the mean-square gyration radius of the trees. By construction, $\nu = \rho \nu_{\text{path}}$, and the relation $\epsilon = \rho$ is expected to hold in general [31]. For ideal, non-interacting trees $\rho = \epsilon = \nu_{\text{path}} = 1/2$ and $\nu = 1/4$ [15, 19]. For interacting systems, the only exactly known exponent is $\nu = 1/2$ for self-avoiding trees in $d = 3$ dimensions [17]. Otherwise, Flory theory [4, 11–14] provides a useful, although approximate, framework for discussing the *average* behavior, Eqs. (1) to (4), of a wide range of interacting tree systems beyond the small number of available exact results [15–17].

The non-Gaussian nature of distribution functions for the above mentioned observables can be investigated by a combination of computer simulations and scaling arguments [18]. The branching statistics is in good agreement with a generalized Kramers form,

$$p_{br}(N_{br}) \approx \left(\frac{N_{br}(N - N_{br})}{N} \right)^{-(2-\epsilon)} N_{br}^{\ll N} N_{br}^{-(2-\epsilon)}. \quad (5)$$

The end-to-end vector distributions, $p_N(\vec{r}|L) \equiv P_N(|\vec{r}| | L) / \frac{2\pi^{d/2} |\vec{r}|^{d-1}}{\Gamma(d/2)}$, for paths of length L on trees of mass N can be approximated as

$$p_N(\vec{r}|L) = \frac{1}{\langle R^2(L) \rangle_N^{d/2}} q \left(\frac{\vec{r}}{\sqrt{\langle R^2(L) \rangle_N}} \right). \quad (6)$$

Here, $\Gamma(z)$ denotes the Euler's gamma function, $\vec{x} = \vec{r} / \sqrt{\langle R^2(L) \rangle_N}$ is the scaled distance and

$$q(\vec{x}) = C |\vec{x}|^{\theta_{\text{path}}} \exp(-K |\vec{x}|^{t_{\text{path}}}) \quad (7)$$

is of the Redner-des Cloizeaux (RdC) [32, 33] form. The shape of the rescaled distributions, and hence the characteristic exponents θ_{path} and t_{path} controlling the small and large distance behaviors respectively, depend on the universality class. While θ_{path} is an independent exponent, t_{path} can be estimated using the Fisher-Pincus relation [34, 35]

$$t_{\text{path}} = \frac{1}{1 - \nu_{\text{path}}}. \quad (8)$$

The constants

$$C = t \frac{\Gamma(1 + \frac{d}{2}) \Gamma(\frac{d+\theta}{2}) (\frac{2+d+\theta}{t})}{d \pi^{d/2} \Gamma(\frac{2+d+\theta}{2}) (\frac{d+\theta}{t})} \quad (9)$$

$$K^2 = \frac{\Gamma(\frac{2+d+\theta}{t})}{\Gamma(\frac{d+\theta}{t})} \quad (10)$$

are determined by the conditions (1) that the distribution is normalized ($\int q(\vec{x}) d\vec{x} \equiv 1$) and (2) that the second moment was chosen as the scaling length ($\int |x|^2 q(\vec{x}) d\vec{x} \equiv 1$).

D. Tight wrapping of ring polymers

The wrapping procedure for trees with a maximal functionality of $f = 3$ [5] is schematically described in

Fig. 1(b). We start from a randomly chosen tip (numbered as “0” in the figure) and construct the ring by adding new bonds consecutively following the branched structure. At a branching point (say, the one marked by the number “2”) we choose randomly between one of the two possible directions and continue placing new bonds until the corresponding branch has been fully travelled by the double-folded path. Once we return to the branching point, we continue along the direction which was not selected in the first instance. Finally, we return to the origin and close the ring. It is easy to see that this procedure ensures that each tree segment is visited exactly twice by oppositely oriented ring segments and that $\ell_{\text{ring}} = 2N$ for the ring contour length. For a given tree, there are 2^{n_3} possible wrappings, where n_3 is the total number of branching nodes of the tree. Here we always consider averages over tree *ensembles*, where we analyse a single randomly generated wrapping per stored tree conformation.

III. RESULTS AND DISCUSSION

A. Tree contour distance as a function of ring contour distance

The central quantity for understanding the conformational statistics of wrapped rings is the average tree contour distance, L , between two monomers as a function of their ring contour distance, ℓ . In general, $L \leq \ell$. The minimal extension, $L = 0$, corresponds to the case, where the ring wraps a branch of the tree composed of $\ell/2$ tree segments. To reach the maximal extension, $L = \ell$, the ring has to follow a linear path of length ℓ on the tree. In general, the part of the tree wrapped by the ring section is in itself a tree composed of $\mathcal{O}(\ell)$ segments. Adapting Eq. (2), we thus expect

$$\lim_{N \rightarrow \infty} \langle L(\ell) \rangle_N \sim \ell^\rho. \quad (11)$$

Furthermore, due to the ring closure $\langle L(\ell) \rangle \equiv \langle L(\ell_{\text{ring}} - \ell) \rangle$ reaches its maximum for $\ell = \ell_{\text{ring}}/2$ before reducing to zero at the total ring size, $\langle L(\ell_{\text{ring}}) \rangle \equiv 0$. The simplest functional form accounting for this constraint is

$$\langle L(\ell) \rangle_N \sim \left(\ell \left(1 - \frac{\ell}{\ell_{\text{ring}}} \right) \right)^\rho. \quad (12)$$

Panels (a) in Figs. 2 to 5 show good agreement with this ansatz. Data are shown for ring contour distances up to $\ell_{\text{ring}}/2$; plotting them as a function of $\ell \left(1 - \frac{\ell}{\ell_{\text{ring}}} \right)$ effectively reduces finite ring size effects (in the insets the same data are shown as a function of ℓ). The dashed lines indicate the expected power law, where we used the effective exponents we extracted [19, 20] for the trees underlying the present ring constructions.

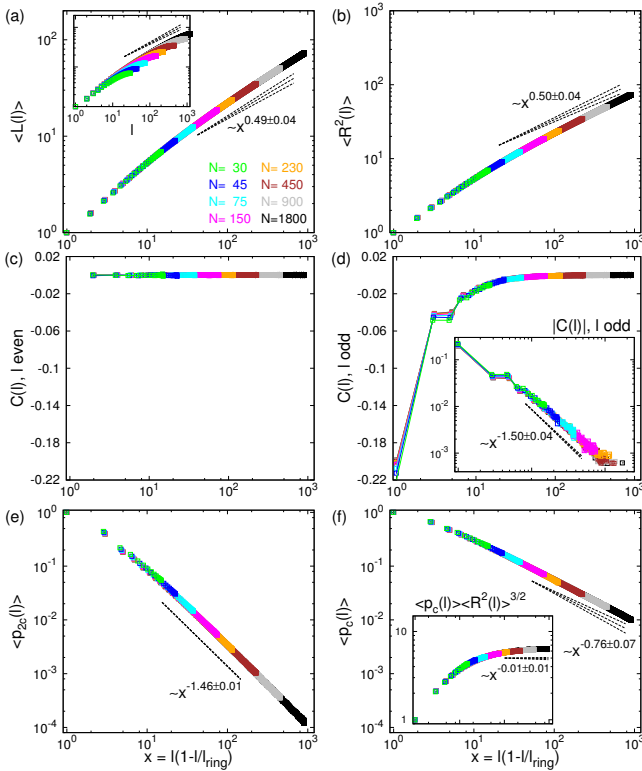


FIG. 2: Conformational statistics of double-folded rings on $3d$ ideal randomly branching trees made of N Kuhn segments. (a) $\langle L(\ell) \rangle \sim \ell^\rho$, average tree contour distance for ring contour distance ℓ ; (b) $\langle R^2(\ell) \rangle \sim \ell^{2\nu}$, end-to-end mean-square spatial distances; (c, d) $C(\ell) \sim \ell^{-2(1-\nu)}$, bond orientation correlation function. In the insets here and in panels (c, d) in Fig. 3 to Fig. 5 data with relative errors $> 20\%$ are considered below noise level and discarded from the plots; (e) $\langle p_{2c}(\ell) \rangle \sim \ell^{-(2-\epsilon)}$, average probability of secondary structure contacts. The straight lines shown in these panels are calculated based on the average values and error bars of scaling exponents ρ , ν and ϵ presented in our works [19, 20]. (f) $\langle p_c(\ell) \rangle \sim \ell^{-\nu(d+\theta_r)}$, contact probability. The straight line is obtained by using the average value and error bars for the scaling exponent θ_r presented in this work, see Table I.

B. Secondary structure contacts

We define as a secondary structure contact a pair of monomers, which are neighbors on the tree, $L_{ij} \leq l_K$, but not along the ring, $|j - i| > 1$ (Fig. 1(b)). We chose a finite contact distance to preserve the analogy with tertiary structure contacts (see below) and evaluated the contact probability $\langle p_{2c}(\ell) \rangle$ only for odd values of ℓ to avoid even/odd fluctuations induced by the lattice. Modulo the finite contact radius, the probability to create a secondary structure contact at a ring distance ℓ equals (symbols *vs.* dashed lines) the probability to cut a branch of size $\ell/2$ from the tree: $\langle p_{2c}(\ell) \rangle = p_{br}(\ell/2)$.

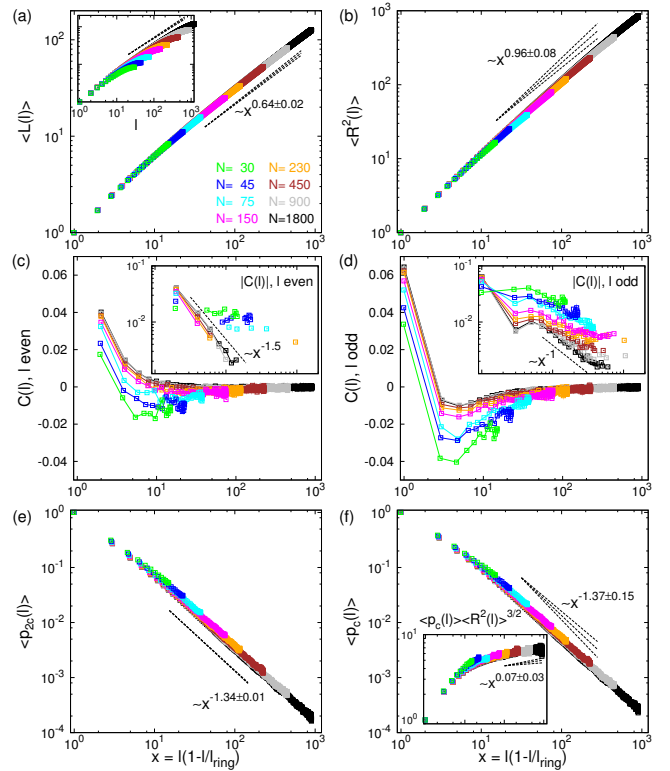


FIG. 3: Conformational statistics of double-folded rings on $3d$ self-avoiding randomly branching trees made of N Kuhn segments. Notation and symbols are as in Fig. 2, except for the *exact* straight lines $\sim \ell^{-1.5}$ and $\sim \ell^{-1}$ in the insets of panels (c) and (d).

In particular, Eq. (5) suggests

$$\lim_{N \rightarrow \infty} \langle p_{2c}(\ell) \rangle_N \sim \ell^{-(2-\epsilon)} \quad (13)$$

$$\langle p_{2c}(\ell) \rangle_N \sim \left(\ell \left(1 - \frac{\ell}{\ell_{ring}} \right) \right)^{-(2-\epsilon)}. \quad (14)$$

Panels (e) in Figs. 2 to 5 show that this is well supported by our data.

C. Tree contour distance distributions

The mean tree contour distance and the secondary structure contact probability can both be obtained from the full tree contour distance distribution, $p_N(L|\ell)$, for ring sections of length ℓ on rings composed of $2N$ Kuhn segments:

$$\langle L(\ell) \rangle_N = \int_0^L L p_N(L|\ell) dL \quad (15)$$

$$\langle p_{2c}(\ell) \rangle_N = \int_0^{\ell_K} p_N(L|\ell) dL \quad (16)$$

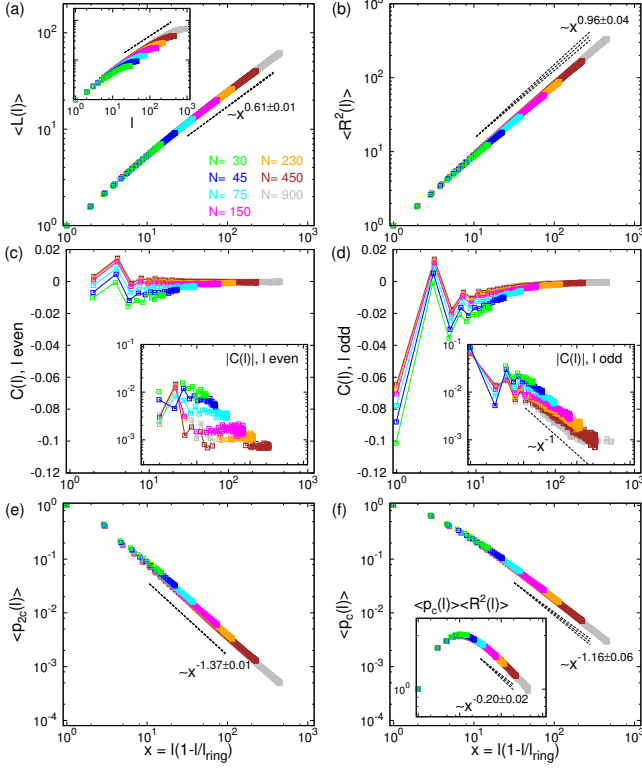


FIG. 4: Conformational statistics of double-folded rings on 2d melt of randomly branching trees made of N Kuhn segments. Notation and symbols are as in Fig. 2, except for the *exact* straight line $\sim \ell^{-1}$ in the inset of panel (d).

Figure 6 shows, that the measured contour distance distributions fall onto universal master curves, when plotted as a function of the rescaled contour distance $x = L/\langle L(\ell) \rangle_N$:

$$p_N(L|\ell) = \frac{1}{\langle L(\ell) \rangle_N} q\left(\frac{L}{\langle L(\ell) \rangle_N}\right). \quad (17)$$

These master curves are well described by the one-dimensional Redner-des Cloizeaux (RdC) form (orange lines in Fig. 6):

$$q(x) = C_L x^{\theta_L} \exp(-K_L x^{t_L}). \quad (18)$$

The constants

$$C_L = t_L \frac{\Gamma^{\theta_L+1}((\theta_L+2)/t_L)}{\Gamma^{\theta_L+2}((\theta_L+1)/t_L)} \quad (19)$$

$$K_L = \frac{\Gamma((\theta_L+2)/t_L)}{\Gamma((\theta_L+1)/t_L)} \quad (20)$$

follow from the conditions that $p_N(L|\ell)$ is normalized to 1 and that the first moment, $\langle L(\ell) \rangle_N$, is the only relevant scaling variable. Estimated values for (θ_L, t_L) in the asymptotic ($N \rightarrow \infty$) limit of large trees are summarized in Table I. More details concerning best fits of Eq. (18) to

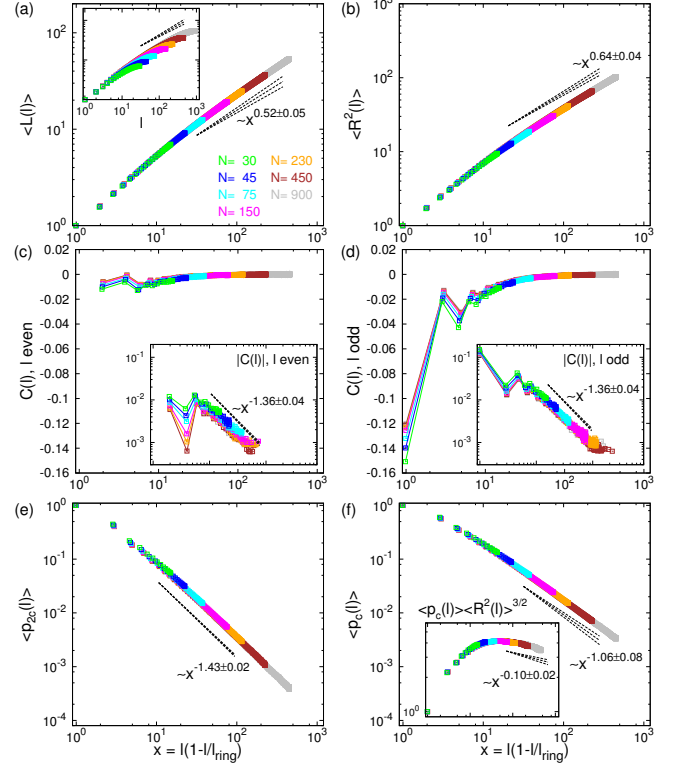


FIG. 5: Conformational statistics of double-folded rings on 3d melt of randomly branching trees made of N Kuhn segments. Notation and symbols are as in Fig. 2.

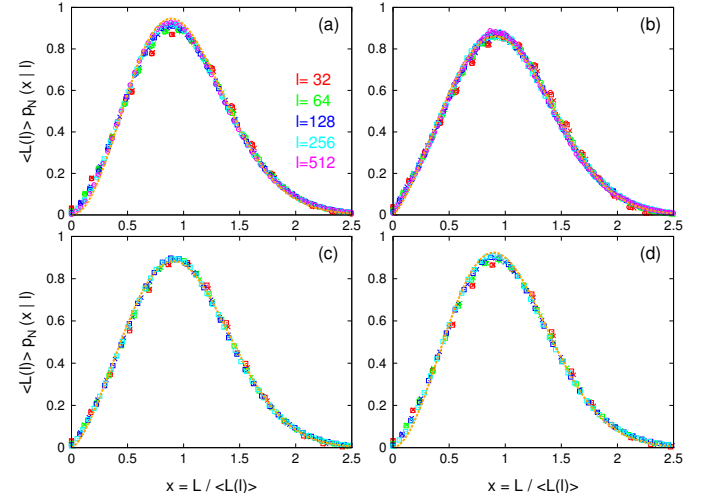


FIG. 6: Rescaled probability distributions, $p_N(L|\ell)$, Eq. (17), of tree contour distances, L , for given ring contour distance ℓ . Different symbols correspond to different tree sizes: (\times) $N = 450$, (\square) $N = 900$, (\circ) $N = 1800$. Results for: (a) 3d ideal trees; (b) 3d self-avoiding trees; (c) 2d melt of trees; (d) 3d melt of trees. Orange lines in panels (a-d) are for best fits (see Table I) to the Redner-des Cloizeaux (RdC) function, Eq. (18).

data for specific values of N and large- N extrapolations of scaling exponents are given in the Appendices and in Table II.

As for the corresponding path length distribution for trees [18], we can give a physical interpretation of the observed (effective) exponents. For small tree contour distances, $x \rightarrow 0$, Eq. (18) reduces to $q(x) = C_L x^{\theta_L}$. Inserting into Eq. (16) for the secondary structure contact probability and equating with Eq. (13) yields:

$$\theta_L = \frac{2}{\rho} - 2. \quad (21)$$

Using the numerical estimates for ρ from Refs. [19, 20], Eq. (21) is in agreement with the extrapolated values for θ_L in the limit $\ell \rightarrow \infty$, see Table I and the Appendices for numerical details. Moreover, note that θ_L differs from the corresponding exponent $\theta_l = \frac{1}{\rho} - 1$ for the contour distance distribution on trees introduced in Ref. [18].

To estimate the probability for observing large contour distances, L , we can follow Ref. [18] and formulate the problem in terms of Pincus blobs [35]. Ring sections, that follow an almost linear path on the tree, behave as if they would wrap a string of ℓ/g unperturbed trees of size $\xi \sim g^\rho$. This suggests that

$$t_L = \frac{1}{1 - \rho}. \quad (22)$$

As for the exponents θ_L , this equation is in reasonable agreement with numerical extrapolations of t_L in the limit $\ell \rightarrow \infty$, see Table I and the Appendices for numerical details.

D. Mean square spatial distances along the ring

Having obtained a complete characterization of wrapping on the level of the connectivity graph characterising the tree, we can now turn our attention to the spatial embedding of the wrapped ring. The simplest measure to consider is the mean-square spatial distance, $\langle R^2(\ell) \rangle_N$, of monomers separated by a contour distance ℓ along the ring. Combining Eqs. (3) and (12) with the relation $\nu = \rho \nu_{\text{path}}$ suggests

$$\langle R^2(\ell) \rangle_N \sim \left(\ell \left(1 - \frac{\ell}{\ell_{\text{ring}}} \right) \right)^{2\nu}. \quad (23)$$

This equation is supported by corresponding numerical results (symbols *vs.* dashed lines) shown in panels (b) in Figs. 2 to 5, where $\nu = 1/4$ for ideal trees, $\nu = 1/2$ for self-avoiding trees in $d = 3$ dimensions, and $\nu = 1/d$ for tree melts in d dimensions.

E. Bond orientation correlation function

Additional insight into the polymer conformation can be gained by considering the bond orientation correlation

function, $C(\ell) = \langle \vec{b}_i \cdot \vec{b}_{i+\ell} \rangle / |\vec{b}|^2$. $C(\ell)$ is related to the mean-square distances via the identity:

$$\begin{aligned} \langle R^2(\ell) \rangle &= 2 \int_0^\ell \int_s^\ell C(s' - s) ds' ds \\ &= 2 \int_0^\ell (\ell - \delta) C(\delta) d\delta \end{aligned} \quad (24)$$

and

$$C(\ell) = \frac{1}{2} \frac{d^2}{d\ell^2} \langle R^2(\ell) \rangle. \quad (25)$$

For $\nu \neq 1/2$, Eq. (25) implies

$$C(\ell) \sim 2\nu(2\nu - 1)\ell^{2(\nu-1)}. \quad (26)$$

In particular, $C(\ell) < 0$ for $\nu < 1/2$. The case $\nu = 1/2$ is special. The best-known examples are: $C(\ell) \equiv 0$ for $\ell > 0$ (Kuhn model or freely jointed chain [10]) and $C(\ell) \equiv \exp(-2\ell/l_K)$ (worm-like chain [36]). However, Eqs. 24 and 25 are also compatible with a power-law decay, $C(\ell) \sim \ell^{-\omega}$, as long as $\omega > 1 = (2 - 2\nu)$. An interesting example are long-range bond orientation correlations in polymer melts [37], where $\omega = 3/2$.

For tightly wrapped rings of the type considered here, it turns out to be useful to distinguish even and odd ring contour distances. Consider first ideal trees, where there is no orientation correlation between different tree segments. As ring segments with arbitrary even $\ell = |j - i| > 0$ can never be co-localized on the same tree segment, $C(\ell) \equiv 0$ for even ℓ (panel (c) in Fig. 2). In contrast, ring segments with odd $\ell = |j - i|$ located on the *same* tree segment are *anti*-correlated. Using Eq. (13) this implies $C(\ell) \sim -\ell^{-(2-\epsilon)} = -\ell^{-3/2}$ for odd ℓ (panel (d) in Fig. 2). This power law is compatible with Eq. (26) as $\nu = 1/4$ for ideal trees [15].

For interacting trees, the bond orientation correlation function exhibits corresponding even/odd fluctuations (panels (c) and (d) in Figs. 3 to 5). In qualitative agreement with the ideal case, distant bonds along the ring have a tendency to be anti-correlated, $C(\ell) < 0$ for $\ell \gg 1$. For rings wrapped around trees from $3d$ melts with $\nu = 1/3$, our results are again in agreement with the power law decay expected from Eq. (26): $C(\ell) \sim -\ell^{2(\nu-1)} = -\ell^{-4/3}$. The bond orientation correlation functions for rings wrapped around trees from $2d$ melts as well as self-avoiding trees with $\nu = 1/2$ are compatible with a convergence to an asymptotic power law decay, $C(\ell) \sim \ell^{-\omega}$, with an exponent, $\omega \approx 1$, close to the limiting value.

F. Tertiary structure contacts and total contacts

We define as a tertiary structure contact a pair of monomers, which are neighbors in space, $|\vec{r}_{ij}| \leq l_K$, but neither on the tree, $L_{ij} > l_K$, nor along the ring,

	Relation to other exponents	3d ideal trees		3d self-avoiding trees		2d melt of trees		3d melt of trees	
		(a)	(b)	(a)	(b)	(a)	(b)	(a)	(b)
θ_L	$\frac{2}{\rho} - 2$	2.05 ± 0.09	2.08 ± 0.34	1.33 ± 0.06	1.13 ± 0.10	1.47 ± 0.06	1.26 ± 0.04	1.82 ± 0.06	1.85 ± 0.37
t_L	$\frac{1}{1-\rho}$	2.01 ± 0.11	1.96 ± 0.15	2.51 ± 0.09	2.78 ± 0.15	2.43 ± 0.08	2.58 ± 0.05	2.15 ± 0.08	2.08 ± 0.22
θ_r	$\min(\theta_{path}, \frac{2-\rho}{\nu} - d)$	0.02 ± 0.05	0	-0.14 ± 0.07	-0.17 ± 0.28	0.42 ± 0.02	0.63 ± 0.04	0.31 ± 0.05	0.28 ± 0.01
t_r	$\frac{1}{1-\nu}$	1.34 ± 0.07	1.33 ± 0.04	2.00 ± 0.06	1.92 ± 0.15	1.90 ± 0.06	1.92 ± 0.07	1.53 ± 0.02	1.47 ± 0.04

TABLE I: Scaling exponents (θ_L, t_L) and (θ_r, t_r) for RdC distribution functions, Eqs. (18) and (31). Columns denoted by (a) and (b) correspond to, respectively, asymptotic values in the infinite ($N \rightarrow \infty$) tree limit and after substitution of values for scaling exponents ρ, ν and θ_{path} obtained in Refs. [18–20] into the relations summarized in this table. For details on the derivation, see Tables II and III in the Appendices.

$|j - i| > 1$ (Fig. 1(b)). Clearly, the sum of both, secondary (see Sec. III B) and tertiary contact probabilities, produces the total contact probability, $\langle p_c(\ell) \rangle$, between pair of ring monomers at contour distance ℓ . Our data for $\langle p_c(\ell) \rangle$ for the various tree types are shown in panels (f) in Figs. 2 to 5. As for secondary structure contacts probabilities, Eq. (14), we can take into account the ring closure constraint through the ansatz

$$\langle p_c(\ell) \rangle_N \sim \left(\ell \left(1 - \frac{\ell}{\ell_{ring}} \right) \right)^{-\gamma_r}, \quad (27)$$

which effectively reduces finite ring-size effects.

G. End-to-end distance distributions for ring sections

The mean square internal distances and the contact probability can both be obtained from the full end-to-end distance distribution, $p_N(\vec{r}|\ell)$, for ring sections of length ℓ on rings composed of $2N$ Kuhn segments:

$$\langle R^2(\ell) \rangle_N = \int_0^\infty |\vec{r}|^2 p_N(\vec{r}|\ell) d\vec{r} \quad (28)$$

$$\langle p_c(\ell) \rangle_N = \int_0^{\ell_K} p_N(\vec{r}|\ell) d\vec{r} \quad (29)$$

Figure 7 shows, that the measured end-to-end distance distributions fall onto universal master curves, when plotted as a function of the rescaled distance $\vec{x} = \vec{r} / \sqrt{\langle R^2(\ell) \rangle_N}$:

$$p_N(\vec{r}|\ell) = \frac{1}{\langle R^2(\ell) \rangle_N^{d/2}} q \left(\frac{\vec{r}}{\sqrt{\langle R^2(\ell) \rangle_N}} \right). \quad (30)$$

These master curves are well described by the d -dimensional Redner-des Cloizeaux (RdC) form (orange lines in Fig. 7):

$$q(\vec{x}) = C |\vec{x}|^{\theta_r} \exp(-K|\vec{x}|^{t_r}) \quad (31)$$

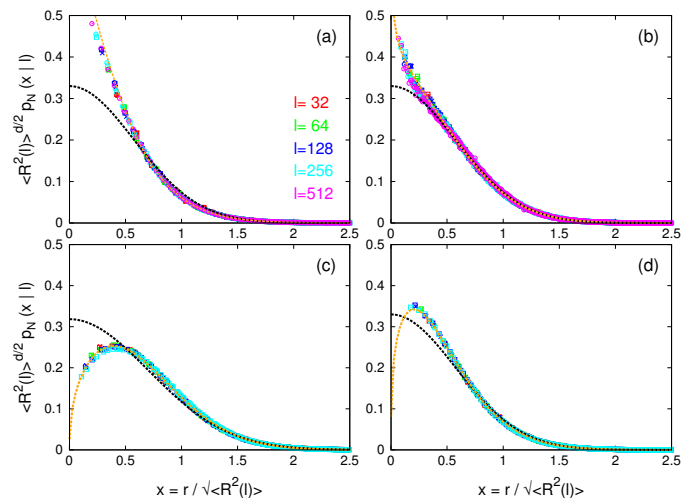


FIG. 7: Probability distribution functions, $p_N(\vec{r}|\ell)$, of end-to-end spatial distances, r , for given ring contour distance ℓ . Notation and symbols are as in Fig. 6. Orange lines in panels (a-d) are for best fits (see Table I) to the RdC function, Eq. (31). Black lines are for the d -dimensional Gaussian function.

with the constants C and K given by Eqs. (9) and (10). In particular, the contact exponent defined in Eq. (27) is given by

$$\gamma_r = \nu(d + \theta_r). \quad (32)$$

Estimated values for (θ_r, t_r) in the asymptotic ($N \rightarrow \infty$) limit of large trees are given in Table I. More details concerning best fits of Eq. (31) to data for specific values of N and large- N extrapolations of scaling exponents are given in the Appendices and in Table III.

In the following, we relate the characteristic exponents θ_r and t_r to our previous results by using Eqs. (7) and (18) together with the identity

$$p_N(\vec{r}|\ell) = \int_0^\infty p_N(\vec{r}|L) p_N(L|\ell) dL, \quad (33)$$

which states that the probability for reaching a particular spatial distance \vec{r} at given ring contour distance ℓ can be calculated by adding up the contributions from all possible tree contour distances, $0 \leq L \leq \ell$. The behavior of $p_N(\vec{r}|\ell)$ for large distances, $r > \sqrt{\langle R^2(\ell) \rangle_N}$, can be estimated from the contour distance $L^*(r)$, which makes the dominant contribution to particle pairs found at the spatial distance r . Combining the arguments of the compressed exponentials in Eqs. (7) and (18), this requires the minimization of $\left(\frac{L}{\langle L(\ell) \rangle_N}\right)^{t_L} + \left(\frac{r}{\sqrt{\langle R^2(L) \rangle_N}}\right)^{t_{path}}$ and yields

$$t_r = \frac{t_L t_{path}}{t_L + t_{path} \nu_{path}} = \frac{1}{1 - \nu}. \quad (34)$$

By using the numerical estimates for ν from our works [19, 20], Eq. (34) is in good agreement with the extrapolated values for t_r (see Table I and the Appendices for numerical details).

In the opposite limit of small distances, $r < \sqrt{\langle R^2(\ell) \rangle_N}$, the exponentials in Eqs. (7) and (18) can be set equal to one in between $L_{min} \sim r^{1/\nu_{path}}$ and $L_{max} \sim L^\rho$. Contributions to the integral Eq. (33) from outside of the interval $[L_{min}, L_{max}]$ are negligible, so that the integral is of the form $\int_{L_{min}}^{L_{max}} L^{-\alpha} dL \stackrel{\alpha \neq 1}{=} (\alpha - 1) (L_{min}^{1-\alpha} - L_{max}^{1-\alpha})$ with $\alpha = \nu_{path}(\theta_{path} + d) - \theta_L$. Depending on the value of α , the integral is dominated by the lower or the upper cutoff for L .

For $\alpha < 1$, the integral is dominated by contributions from long paths with $\langle R^2(L) \rangle_N \gg r^2$. By using values for ν_{path} and θ_{path} from our works [18–20] and θ_L from this work (Table I), this is the case for rings wrapping ideal trees ($\alpha = -0.52 \pm 0.12$), rings wrapping trees from 2d and 3d melts ($\alpha = 0.58 \pm 0.10$ and $\alpha = 0.13 \pm 0.09$, respectively). The only r -dependence comes through the explicit $r^{\theta_{path}}$ term and hence

$$\theta_r = \theta_{path} \quad \text{if} \quad \theta_{path} < \frac{2 - \rho}{\nu} - d. \quad (35)$$

This is borne out by our data (symbols *vs.* dashed lines in panels (f) in Figs. 2, 4, and 5). In these cases, the total contact probability exceeds by far the secondary structure contact probability (*cf.* the corresponding panels (e)).

In the opposite limit, short paths dominate and the total contact probability is essentially given by the secondary structure contact probability. Of the systems we have studied, only rings wrapped around self-avoiding trees in $d = 3$ dimensions fall into this category ($\alpha = 1.68 \pm 0.20$, panels (e) and (f) in Figs. 3). In this case,

$$\theta_r = \frac{2 - \rho}{\nu} - d \quad \text{if} \quad \frac{2 - \rho}{\nu} - d < \theta_{path} \quad (36)$$

in agreement with Eqs. (13) and (32). Summarizing,

$$\theta_r = \min(\theta_{path}, \frac{2 - \rho}{\nu} - d). \quad (37)$$

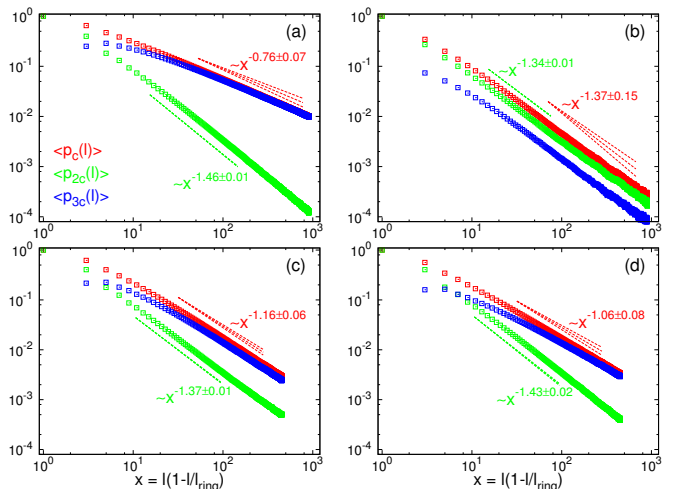


FIG. 8: Secondary structure ($\langle p_{2c}(\ell) \rangle$), tertiary structure ($\langle p_{3c}(\ell) \rangle$) and generic contact probabilities ($\langle p_c(\ell) \rangle = \langle p_{2c}(\ell) \rangle + \langle p_{3c}(\ell) \rangle$) between ring monomers for contour length separation ℓ (see Fig. 1(b) for definitions). Dashed lines are for the expected scaling behaviors $\langle p_{2c}(\ell) \rangle \sim \ell^{-(2-\epsilon)}$ and $\langle p_c(\ell) \rangle \sim \ell^{-\nu(d+\theta_r)}$, as in panels (e) and (f) of Figs. 2 to 5. Results for: (a) 3d ideal trees ($N = 1800$); (b) 3d self-avoiding trees ($N = 1800$); (c) 2d melt of trees ($N = 900$); (d) 3d melt of trees ($N = 900$).

Once again Eq. (37) is in good agreement with the fitted values for θ_r (see Table I and the Appendices for numerical details), if we use the numerical values for ρ , ν and θ_{path} from Refs. [18–20]. However, as illustrated by Fig. 8, the prefactors of these power laws also matter. For rings wrapped around trees from, in particular, 3d melts (panel (d)), the relative weight of the contributions of secondary and tertiary structure contacts to $\langle p_c(\ell) \rangle_N$ is a function of ring contour distance, ℓ , giving rise to a small crossover with contact probabilities being described by intermediate effective exponents.

IV. CONCLUSIONS

The mapping to lattice trees [1, 2] presents an elegant simplification for a polymer problem that is otherwise difficult to treat: the conformation of ring polymers constrained by the absence of topological links with each other or a lattice of obstacles representing the gels used in electrophoresis. The statistical physics of lattice trees can be studied within Flory theory [14]. Computer simulations and scaling arguments allow to refine the values of exponents and to explore the distribution functions characterising tree behavior beyond the average regime [18].

The results we have presented in this article show, that it is relatively straightforward (albeit not completely trivial) to transfer results obtained for trees to the original ring systems. “Navigating” on the tree along a wrapped

ring mixes the two basic concepts used for characterizing trees. The branching statistics of the trees controls the central quantity for understanding the conformational statistics of wrapped rings: the increase of the tree contour distance, $\langle L(\ell) \rangle \sim \ell^\rho$, between two monomers as a function of their ring contour distance, ℓ . Spatial distances depend on the conformations of linear paths on the tree in the embedding space. Using $\langle R^2(L) \rangle \sim L^{2\nu_{path}}$ with $\nu = \rho\nu_{path}$ for trees, one recovers for wrapped rings the familiar relation $\langle R^2(\ell) \rangle \sim \ell^{2\nu}$. The ring closure constraint is effectively dealt with by expressing observables

as a function of $\ell(1 - \ell/\ell_{ring})$. Interestingly, the distribution functions $p(\vec{r}|\ell)$ and $p(L|\ell)$ for the spatial distance, \vec{r} , and tree contour distance, L , between monomers show excellent scaling behavior when expressed as a function of reduced spatial and contour distance, $\vec{r}/\sqrt{\langle R^2(\ell) \rangle}$ and $L/\langle L(\ell) \rangle$. As for trees [18], the scaled distributions turn out to be of the Redner-des Cloizeaux form [32, 33]. They are characterized by two exponents, t and θ , which control the small and the large-scale behavior and which can be related to the other exponents describing rings and the trees they are wrapped around.

-
- [1] A. R. Khokhlov and S. K. Nechaev, *Phys. Lett.* **112A**, 156 (1985).
- [2] M. Rubinstein, *Phys. Rev. Lett.* **57**, 3023 (1986).
- [3] S. P. Obukhov, M. Rubinstein, and T. Duke, *Phys. Rev. Lett.* **73**, 1263 (1994).
- [4] A. Y. Grosberg, *Soft Matter* **10**, 560 (2014).
- [5] A. Rosa and R. Everaers, *Phys. Rev. Lett.* **112**, 118302 (2014).
- [6] J. Smrek and A. Y. Grosberg, *J. Phys.-Condens. Matter* **27**, 064117 (2015).
- [7] D. Michieletto, *Soft Matter* **12**, 9485 (2016).
- [8] B. Alberts et al., *Molecular Biology of the Cell* (Garland Science, New York, 2007), 5th ed.
- [9] M. Doi and S. F. Edwards, *The Theory of Polymer Dynamics* (Oxford University Press, New York, 1986).
- [10] M. Rubinstein and R. H. Colby, *Polymer Physics* (Oxford University Press, New York, 2003).
- [11] J. Isaacson and T. C. Lubensky, *J. Physique Lett.* **41**, L469 (1980).
- [12] M. Daoud and J. F. Joanny, *J. Physique* **42**, 1359 (1981).
- [13] A. M. Gutin, A. Y. Grosberg, and E. I. Shakhnovich, *Macromolecules* **26**, 1293 (1993).
- [14] R. Everaers, A. Y. Grosberg, M. Rubinstein, and A. Rosa, *Soft Matter* **13**, 1223 (2017).
- [15] B. H. Zimm and W. H. Stockmayer, *J. Chem. Phys.* **17**, 1301 (1949).
- [16] P.-G. De Gennes, *Biopolymers* **6**, 715 (1968).
- [17] G. Parisi and N. Sourlas, *Phys. Rev. Lett.* **46**, 871 (1981).
- [18] A. Rosa and R. Everaers, *Phys. Rev. E* **95**, 012117 (2017).
- [19] A. Rosa and R. Everaers, *J. Phys. A: Math. Theor.* **49**, 345001 (2016).
- [20] A. Rosa and R. Everaers, *J. Chem. Phys.* **145** (2016).
- [21] M. Kapnistos et al., *Nature Materials* **7**, 997 (2008).
- [22] D. Michieletto, D. Marenduzzo, E. Orlandini, and M. S. Turner, *Polymers* **9**, 349 (2017).
- [23] M. E. Cates and J. M. Deutsch, *J. Phys. (Paris)* **47**, 2121 (1986).
- [24] T. Ge, S. Panyukov, and M. Rubinstein, *Macromolecules* **49**, 708 (2016).
- [25] A. Grosberg, Y. Rabin, S. Havlin, and A. Neer, *Europhys. Lett.* **23**, 373 (1993).
- [26] A. Rosa and R. Everaers, *Plos Comput. Biol.* **4**, e1000153 (2008).
- [27] T. Vettorel, A. Y. Grosberg, and K. Kremer, *Phys. Biol.* **6**, 025013 (2009).
- [28] L. A. Mirny, *Chromosome Res.* **19**, 37 (2011).
- [29] M. Lang, *Macromolecules* **46**, 1158 (2013).
- [30] J. Smrek and A. Y. Grosberg, *ACS Macro Letters* **5**, 750 (2016).
- [31] E. J. Janse van Rensburg and N. Madras, *J. Phys. A: Math. Gen.* **25**, 303 (1992).
- [32] S. Redner, *J. Phys. A: Math. Gen.* **13**, 3525 (1980).
- [33] J. des Cloizeaux and G. Jannink, *Polymers in Solution* (Oxford University Press, Oxford, 1989).
- [34] M. E. Fisher, *J. Chem. Phys.* **44**, 616 (1966).
- [35] P. Pincus, *Macromolecules* **9**, 386 (1976).
- [36] O. Kratky and G. Porod, *Rec. Trav. Chim. Pays-Bas.* **68**, 1106 (1949).
- [37] J. P. Wittmer, H. Meyer, J. Baschnagel, A. Johner, S. Obukhov, L. Mattioni, M. Müller, and A. N. Semenov, *Phys. Rev. Lett.* **93**, 147801 (2004).
- [38] W. A. Seitz and D. J. Klein, *J. Chem. Phys.* **75**, 5190 (1981).
- [39] W. H. Press, S. A. Teukolsky, W. T. Vetterling, and B. F. Flannery, *Numerical Recipes in Fortran* (Cambridge University Press, Cambridge, 1992), 2nd ed.

Appendix A: Model and methods

1. Generation of equilibrated conformations of randomly branching trees

Spatial conformations of branched polymers were generated according to the lattice polymer model extensively described in our former works [18–20]. Full details can be found there, here we just provide a concise description of the method.

Briefly, we simulated randomly branching polymers with volume interactions by employing a slightly modified version of the “amoeba” Monte Carlo algorithm [38] for trees on the cubic lattice with periodic boundary conditions. In this model, connected nodes occupy adjacent lattice sites. As there is no bending energy term, the lattice constant equals the Kuhn length, l_K , of linear paths across ideal trees. The functionality of nodes is restricted to the values $f = 1$ (a leaf or branch tip), $f = 2$ (linear chain section), and $f = 3$ (branch point). Here, we consider $3d$ single trees in good solvent (self-avoiding trees), and $2d$ and $3d$ trees in melt with Kuhn density $\rho_K l_K^d = 2$. Tree sizes are in the range $30 \leq N \leq 1800$ for ideal and

self-avoiding trees and $30 \leq N \leq 900$ for trees in melt.

2. Numerical fitting procedures for deriving scaling exponents for Redner-des Cloizeaux functions

Single estimates of scaling exponents (θ_L, t_L) and (θ_r, t_r) for Redner-des Cloizeaux (RdC) functions Eq. (18) and Eq. (31) describing the behavior of distribution functions $p_N(L|\ell)$ and $p_N(\bar{r}|\ell)$ (Figs. 6 and 7, lines *vs.* symbols respectively) are obtained through the following procedure. First, we fit the analytical expressions for the RdC functions to our measured distributions for the largest tree sizes ($N = 450, 900, 1800$) and for specific values of ring contour distances $\ell = 32, 64, \dots, \approx N/4$. Corresponding results for (θ_L, t_L) and (θ_r, t_r) are summarized in Tables II and III, respectively.

As, in general, the effective exponents θ_L and t_L show consistent finite-size effects depending monotonously on ℓ , we have used the empirical expression:

$$\theta_L(\ell) = \theta_L(\infty) + A\ell^{-\Delta} \quad (\text{A1})$$

containing free parameters $\theta_L(\infty)$, A and Δ and an analogous one for $t_L(\ell)$ to estimate asymptotic values, $\theta_L(\infty)$ and $t_L(\infty)$. Per each N a separate fitting procedure has been carried on, leading to different estimates for the asymptotic values. In all cases, the quality of the fits is estimated by standard statistical analysis [39]: normalized χ -square test $\tilde{\chi}^2 \equiv \frac{\chi^2}{D-f}$, where $D-f$ is the difference

between the number of data points, D , and the number of fit parameters, f . The corresponding $\mathcal{Q}(D-f, \chi^2)$ -values provide a quantitative indicator for the likelihood that χ^2 should exceed the observed value, if the model were correct [39]. The results of all fits are reported together with the corresponding errors, $\tilde{\chi}^2$ and \mathcal{Q} values (Table II). The reported value for Δ corresponds to the one giving the smallest $\tilde{\chi}^2$. Our final values for θ_L and t_L (Table II, in boldface) are hence calculated by averaging the separate results for different N 's. Error bars are given as $\sqrt{(\text{statistical error})^2 + (\text{systematic error})^2}$, where the ‘‘statistical error’’ is the largest error bar between different N 's [31] and the ‘‘systematic error’’ is the spread between the single estimates.

Unfortunately, excluding the exceptions of θ_r for ideal trees (all N 's) and for $3d$ self-avoiding trees ($N = 450$), the same strategy applied to the pair (θ_r, t_r) fails (Table III). This is probably related to the fact that finite size effects for θ_r and t_r are, in general, smaller than for the previous exponents. In those cases where the extrapolation procedure does not work, we have then simply taken averages of single estimates for each different N and calculated error bars by the same combination of statistical and systematic errors as described above. Final values for θ_r and t_r (Table III, in boldface) are then computed in the same way as for θ_L and t_L .

Appendix B: Supplementary tables

	3d ideal trees		3d self-avoiding trees		2d melt of trees		3d melt of trees	
(a) θ_L and t_L from best fits of numerical distributions, $p_N(L \ell)$, to the RdC function								
ℓ	θ_L	t_L	θ_L	t_L	θ_L	t_L	θ_L	t_L
$N = 450$								
32	1.250 ± 0.041	2.851 ± 0.094	1.013 ± 0.034	3.459 ± 0.125	1.221 ± 0.041	3.078 ± 0.108	1.223 ± 0.040	2.941 ± 0.098
64	1.478 ± 0.033	2.418 ± 0.053	1.148 ± 0.025	2.878 ± 0.063	1.366 ± 0.034	2.639 ± 0.066	1.426 ± 0.033	2.483 ± 0.056
128	1.632 ± 0.027	2.251 ± 0.035	1.211 ± 0.021	2.698 ± 0.045	1.406 ± 0.026	2.528 ± 0.046	1.555 ± 0.027	2.313 ± 0.038
Δ	0.569	1.374	1.104	1.700	1.862	1.972	0.655	1.436
$\tilde{\chi}^2$	4×10^{-7}	2×10^{-7}	5×10^{-9}	8×10^{-8}	4×10^{-8}	5×10^{-8}	2×10^{-7}	7×10^{-8}
\mathcal{Q}	0.9995	0.9997	0.9999	0.9998	0.9998	0.9998	0.9996	0.9998
$\ell \rightarrow \infty$	1.95 ± 0.06	2.15 ± 0.04	1.27 ± 0.03	2.62 ± 0.05	1.42 ± 0.03	2.49 ± 0.05	1.78 ± 0.05	2.21 ± 0.04
$N = 900$								
32	1.259 ± 0.041	2.845 ± 0.094	1.026 ± 0.032	3.514 ± 0.120	1.248 ± 0.041	3.065 ± 0.106	1.231 ± 0.040	2.937 ± 0.097
64	1.517 ± 0.037	2.370 ± 0.055	1.191 ± 0.026	2.852 ± 0.063	1.409 ± 0.038	2.616 ± 0.070	1.472 ± 0.038	2.432 ± 0.061
128	1.711 ± 0.033	2.135 ± 0.039	1.292 ± 0.025	2.608 ± 0.049	1.523 ± 0.034	2.374 ± 0.050	1.637 ± 0.033	2.203 ± 0.042
256	1.822 ± 0.024	2.053 ± 0.025	1.310 ± 0.017	2.503 ± 0.031	1.499 ± 0.023	2.402 ± 0.036	1.717 ± 0.024	2.137 ± 0.028
Δ	0.571	1.197	1.162	1.366	1.607	1.791	0.741	1.352
$\tilde{\chi}^2$	5×10^{-2}	5×10^{-2}	2×10^{-1}	9×10^{-3}	7×10^{-1}	9×10^{-1}	6×10^{-2}	7×10^{-2}
\mathcal{Q}	0.9509	0.9477	0.7924	0.9906	0.4884	0.4121	0.9462	0.9349
$\ell \rightarrow \infty$	2.07 ± 0.04	1.98 ± 0.03	1.34 ± 0.02	2.44 ± 0.03	1.52 ± 0.02	2.37 ± 0.03	1.85 ± 0.03	2.08 ± 0.03
$N = 1800$								
32	1.265 ± 0.041	2.835 ± 0.093	1.048 ± 0.034	3.502 ± 0.125				
64	1.524 ± 0.037	2.351 ± 0.054	1.214 ± 0.026	2.885 ± 0.062				
128	1.782 ± 0.037	2.042 ± 0.039	1.344 ± 0.025	2.585 ± 0.047				
256	1.922 ± 0.031	1.942 ± 0.029	1.399 ± 0.023	2.473 ± 0.039				
512	1.963 ± 0.021	1.945 ± 0.019	1.359 ± 0.017	2.528 ± 0.031				
Δ	0.651	1.317	1.247	1.575				
$\tilde{\chi}^2$	9×10^{-1}	1×10^0	2×10^0	1×10^0				
\mathcal{Q}	0.4397	0.4122	0.144	0.320				
$\ell \rightarrow \infty$	2.12 ± 0.02	1.91 ± 0.02	1.39 ± 0.01	2.48 ± 0.02				
	2.05 ± 0.09	2.01 ± 0.11	1.33 ± 0.06	2.51 ± 0.09	1.47 ± 0.06	2.43 ± 0.08	1.82 ± 0.06	2.15 ± 0.08
(b) Theoretical predictions $\theta_L = \frac{2}{\rho} - 2$ and $t_L = \frac{1}{1-\rho}$								
	θ_L	t_L	θ_L	t_L	θ_L	t_L	θ_L	t_L
	2.08 ± 0.34	1.96 ± 0.15	1.13 ± 0.10	2.78 ± 0.15	1.26 ± 0.04	2.58 ± 0.05	1.85 ± 0.37	2.08 ± 0.22

TABLE II: Conformational statistics of tree contour distance L at given ring contour distance ℓ . (a) Effective exponents θ_L and t_L obtained by best fits of numerical distributions, $p_N(L|\ell)$ (Fig. 6), to the Redner-des Cloizeaux function, Eq. (18), for different ℓ and tree sizes N . Final estimates and corresponding error bars are highlighted in boldface. (b) Estimates of exponents θ_L and t_L according to the scaling relations Eqs. (21) and (22) and using average values and error bars of exponents ρ from our works [19, 20]: $\rho = 0.49 \pm 0.04$ (3d ideal trees), $\rho = 0.64 \pm 0.02$ (3d self-avoiding trees), $\rho = 0.613 \pm 0.007$ (2d tree melt), $\rho = 0.52 \pm 0.05$ (3d tree melt).

	3d ideal trees		3d self-avoiding trees		2d melt of trees		3d melt of trees	
(a) θ_r and t_r from best fits of numerical distributions, $p_N(\vec{r} \ell)$, to the RdC function								
ℓ	θ_r	t_r	θ_r	t_r	θ_r	t_r	θ_r	t_r
$N = 450$								
32	0.541 ± 0.139	1.251 ± 0.046	-0.106 ± 0.017	1.991 ± 0.020	0.400 ± 0.015	1.870 ± 0.017	0.245 ± 0.034	1.563 ± 0.019
64	0.236 ± 0.057	1.321 ± 0.025	-0.136 ± 0.008	2.001 ± 0.011	0.420 ± 0.009	1.877 ± 0.012	0.265 ± 0.010	1.534 ± 0.006
128	0.113 ± 0.023	1.373 ± 0.012	-0.159 ± 0.006	2.032 ± 0.009	0.396 ± 0.005	1.968 ± 0.007	0.278 ± 0.005	1.536 ± 0.004
Δ	1.309	–	0.435	–	–	–	0.622	–
$\tilde{\chi}^2$	4×10^{-8}	–	8×10^{-9}	–	–	–	4×10^{-9}	–
\mathcal{Q}	0.9998	–	0.9999	–	–	–	0.9999	–
$\ell \rightarrow \infty$	0.03 ± 0.04	1.32 ± 0.07	-0.22 ± 0.02	2.01 ± 0.03	0.41 ± 0.02	1.91 ± 0.05	0.30 ± 0.02	1.54 ± 0.02
$N = 900$								
32	0.464 ± 0.131	1.277 ± 0.046	-0.081 ± 0.019	1.962 ± 0.021	0.409 ± 0.014	1.866 ± 0.015	0.204 ± 0.031	1.595 ± 0.018
64	0.208 ± 0.056	1.332 ± 0.025	-0.087 ± 0.010	1.935 ± 0.013	0.457 ± 0.011	1.821 ± 0.013	0.243 ± 0.008	1.550 ± 0.005
128	0.150 ± 0.024	1.344 ± 0.012	-0.127 ± 0.006	1.979 ± 0.008	0.448 ± 0.007	1.879 ± 0.009	0.287 ± 0.007	1.525 ± 0.005
256	0.077 ± 0.010	1.392 ± 0.006	-0.163 ± 0.005	2.077 ± 0.008	0.421 ± 0.005	1.974 ± 0.007	0.300 ± 0.003	1.524 ± 0.002
Δ	0.735	–	–	–	–	–	0.842	1.590
$\tilde{\chi}^2$	4×10^{-1}	–	–	–	–	–	7×10^{-1}	8×10^{-1}
\mathcal{Q}	0.6962	–	–	–	–	–	0.5000	0.4424
$\ell \rightarrow \infty$	-0.02 ± 0.03	1.34 ± 0.06	-0.11 ± 0.04	1.99 ± 0.06	0.43 ± 0.02	1.89 ± 0.06	0.324 ± 0.005	1.521 ± 0.002
$N = 1800$								
32	0.271 ± 0.117	1.361 ± 0.046	-0.089 ± 0.013	1.991 ± 0.016				
64	0.163 ± 0.050	1.354 ± 0.023	-0.079 ± 0.008	1.939 ± 0.011				
128	0.113 ± 0.021	1.365 ± 0.011	-0.093 ± 0.006	1.960 ± 0.008				
256	0.086 ± 0.009	1.379 ± 0.006	-0.085 ± 0.005	1.988 ± 0.007				
512	0.069 ± 0.004	1.393 ± 0.003	-0.110 ± 0.003	2.065 ± 0.005				
Δ	0.827	–	–	–				
$\tilde{\chi}^2$	9×10^{-3}	–	–	–				
\mathcal{Q}	0.9988	–	–	–				
$\ell \rightarrow \infty$	0.05 ± 0.01	1.37 ± 0.05	-0.09 ± 0.02	1.99 ± 0.05				
	0.02 ± 0.05	1.34 ± 0.07	-0.14 ± 0.07	2.00 ± 0.06	0.42 ± 0.02	1.90 ± 0.06	0.31 ± 0.05	1.53 ± 0.02
(b) Theoretical predictions $\theta_r = \min(\theta_{path}, \frac{2-\rho}{\nu} - d)$ and $t_r = \frac{1}{1-\nu}$								
	θ_r	t_r	θ_r	t_r	θ_r	t_r	θ_r	t_r
	0	1.33 ± 0.04	-0.17 ± 0.28	1.92 ± 0.15	0.63 ± 0.04	1.92 ± 0.07	0.28 ± 0.01	1.47 ± 0.04

TABLE III: Conformational statistics of end-to-end spatial distances of ring sections of linear size ℓ . (a) Effective exponents θ_r and t_r obtained by best fits of numerical distributions, $p_N(\vec{r}|\ell)$ (Fig. 7), to the Redner-des Cloizeaux function, Eq. (31), for different ℓ and tree sizes N . Final estimates and corresponding error bars are highlighted in boldface. (b) Estimates of exponents θ_r and t_r according to the scaling relations Eqs. (34) and (37) and using average values and error bars of exponents ρ (summarized in the caption of Table II), ν and θ_{path} from our works [18–20]: $\nu = 0.25 \pm 0.02$ and $\theta_{path} = 0$ (3d ideal trees), $\nu = 0.48 \pm 0.04$ and $\theta_{path} = 1.07 \pm 0.08$ (3d self-avoiding trees), $\nu = 0.48 \pm 0.02$ and $\theta_{path} = 0.63 \pm 0.04$ (2d tree melt), $\nu = 0.32 \pm 0.02$ and $\theta_{path} = 0.28 \pm 0.01$ (3d tree melt),